Journal of Materials Chemistry C

PAPER

View Article Online
View Journal | View Issue

Cite this: J. Mater. Chem. C, 2017, 5, 2043

Coexistence of long-range ferromagnetic ordering and spin-glass behavior observed in the first inorganic–organic hybrid 1-D oxalate-bridging nona-Mn^{II} sandwiched tungstoantimonate chain†

Jiancai Liu,[a] Jie Luo,[a] Qing Han,[a] Jing Cao,[a] Lijuan Chen,*[a] You Song*[ab] and Junwei Zhao*[ac]

A neoteric 1-D sinusoidal tungstoantimonate (TA) $Na_2H_4\{[Mn(H_2O)_3]_3[Mn(H_2O)_2]_2[Mn(H_2O)][Mn(C_2O_4)]_3$-$[B\text{-}\alpha\text{-}SbW_9O_{33}]_2\}\cdot 31H_2O$ (**1**) was synthesized from the reaction of $Na_9[B\text{-}\alpha\text{-}SbW_9O_{33}]\cdot 19.5H_2O$ with $MnCl_2\cdot 4H_2O$ with the assistance of oxalic acid and structurally characterized by elemental analysis, IR spectroscopy, single-crystal X-ray diffraction, powder X-ray diffraction and thermal analyses. In **1**, an unprecedented oxalate-bridging nona-Mn^{II} $\{[Mn(H_2O)_3]_3[Mn(H_2O)_2]_2[Mn(H_2O)][Mn(C_2O_4)]_3\}^{12+}$ cluster is clamped by two trivacant Keggin $[B\text{-}\alpha\text{-}SbW_9O_{33}]^{9-}$ fragments forming a unique nona-Mn^{II}-encapsulated sandwich-type species. In the sandwich belt, the internal hexa-Mn^{II} $\{[Mn(H_2O)_2]_2[Mn(H_2O)][Mn(C_2O_4)]_3\}^{6+}$ ring is alternately concatenated with three $[Mn(H_2O)_3]^{2+}$ ions situated at three vertices of an equicrural triangle through oxalate linkers, completing an approximately coplanar nona-Mn^{II} core. More interestingly, adjacent nona-Mn^{II}-sandwiched TA units are interconnected by double Mn^{II}–C_2O_4 linkages, giving rise to the first inorganic–organic hybrid 1-D chain high-nuclear Mn-sandwiched TA. Furthermore, the zero-field-cooling/field-cooled magnetization and alternating current magnetic susceptibility measurements reveal the occurrence of long-range ferromagnetic ordering and spin-glass behavior in **1**, which are further consolidated by the fitting of the Arrhenius law and the conventional critical scaling law of spin dynamics.

Received 19th December 2016,
Accepted 18th January 2017

DOI: 10.1039/c6tc05479j

rsc.li/materials-c

Introduction

The continuous exploitation and research of new molecule-based magnetic materials has evoked considerable attention with the development of the information technology revolution on account of their realized and potential applications in high-density information storage, quantum computing and low-temperature magnetic refrigerants.[1] The discovery of magnetic materials with special magnetic phenomena such as single-molecular magnets (SMMs) or single-chain magnets (SCMs) is a prodigious breakthrough and opens up a popular avenue in the field of nanomagnetism. Recent particular emphasis has been placed not only on designing new SMMs or SCMs, but also on exploiting other unique magnetic phenomena and behaviors.

It is well-known that polyoxometalates (POMs), as a kind of well-defined anionic metal-oxo clusters of early transition metals (W, Mo, Nb, or V) in their high oxidation states with remarkable molecular and electronic tunabilities, can function as attracting inorganic multidentate ligands to incorporate almost any metal moiety into the compositions of POMs, rendering them with broad prospects in the construction of novel transition metal (TM)-substituted POMs (TMSPs) and widespread potential applications in catalysis, medicine, molecular magnetism and materials science.[2] It should be further noted that one very intriguing subfamily of TMSPs is the sandwich-type species that is usually constructed from two lacunary POM fragments hinged by a diverse and versatile TM core. To date, the number of TM centers in the sandwich belt within the reported sandwich-type TMSPs (STMSPs) has generally been less than six (Fig. 1),[3–8] principally because the oxygen atoms in the defect sites of lacunary POM moieties are fully coordinated by TM cations and are therefore unable to bind many more TM cations and the

[a] Henan Key Laboratory of Polyoxometalate Chemistry, Institute of Molecular and Crystal Engineering, College of Chemistry and Chemical Engineering, Henan University, Kaifeng, Henan 475004, China. E-mail: zhaojunwei@henu.edu.cn, ljchen@henu.edu.cn

[b] State Key Laboratory of Coordinate Chemistry, Collaborative Innovation Center of Advanced Microstructures, School of Chemistry and Chemical Engineering, Nanjing University, Nanjing 210093, China. E-mail: yousong@nju.edu.cn

[c] State Key Laboratory of Structural Chemistry, Fujian Institute of Research on the Structure of Matter, Chinese Academy of Sciences, Fuzhou, Fujian 350002, China

† Electronic supplementary information (ESI) available: The refinement details and additional figures. CCDC 1513036. For ESI and crystallographic data in CIF or other electronic format see DOI: 10.1039/c6tc05479j

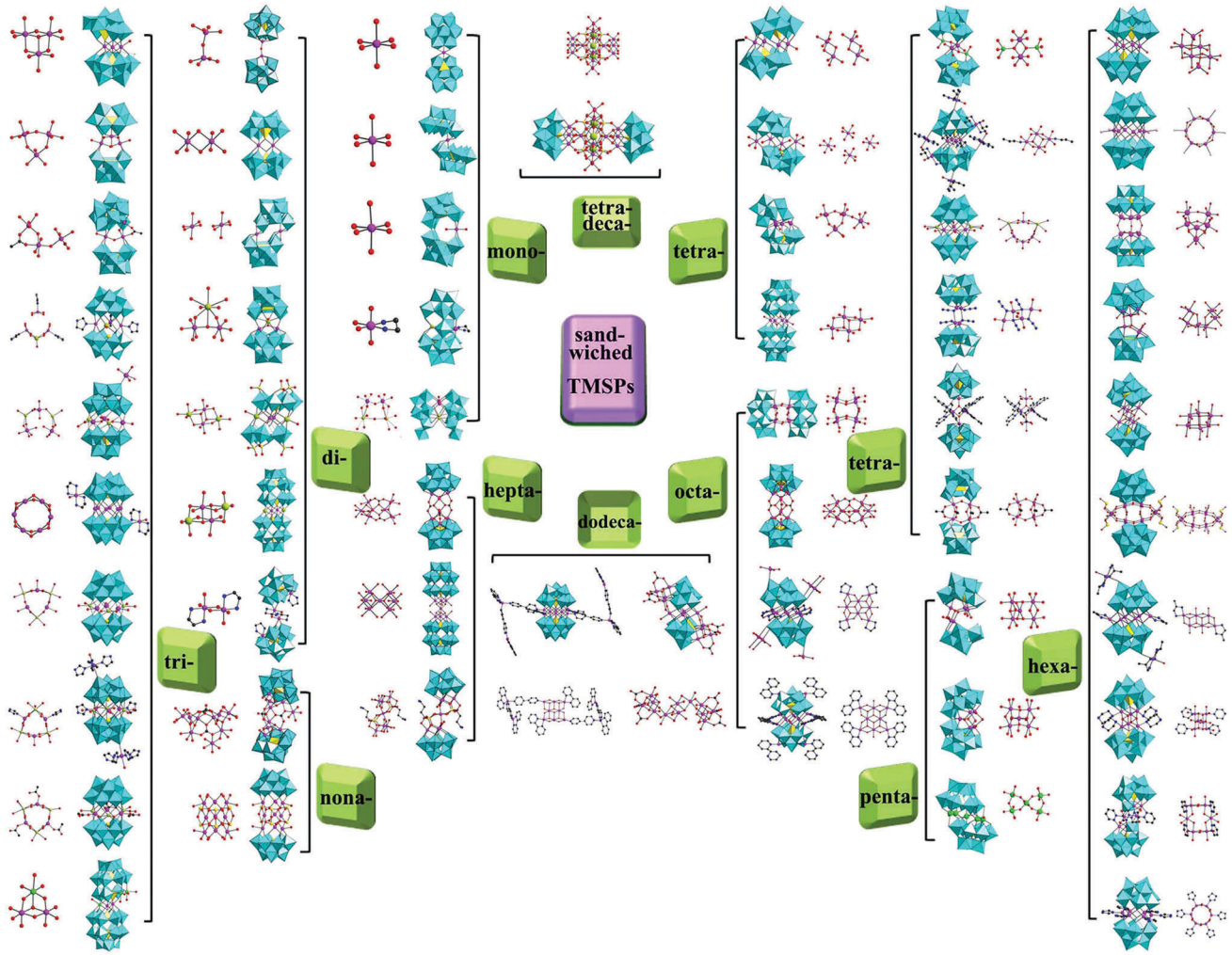

Fig. 1 A summary of some representative sandwiched TMSPs. WO_6 octahedra, turquiose; XO_n polyhedral, yellow; X, yellow; TM, pink; TM′, bright green; Na, K, and Rb, lime; O, red; C, gray-80%; N, blue.

in situ generated higher-nuclear TM clusters in the sandwich belt are unstable without the aid of extraneous structure-stabilizing agents.[9a] As a consequence, discovering and encapsulating higher nuclearity, by increasing the number of TM centers, in the central sandwich belt of STMSPs is always a particularly fascinating area and a long-standing pursuit. Albeit an abundance of STMSPs with various TM nuclearities from 1 to 6 have been prepared and well-documented,[3–8] reports on magnetic STMSP species with TM nuclearityhigher than 7 are scarce, mainly involving heptanuclear $[\{(B\text{-}\alpha\text{-}PW_9O_{34})Co_3(OH)(H_2O)_2(Ale)\}_2Co]^{14-}$ and $[Ni_7(OH)_4(H_2O)(CO_3)_2(HCO_3)(A\text{-}\alpha\text{-}SiW_9O_{34})(\beta\text{-}SiW_{10}O_{37})]^{15-}$,[8f,9b] octanuclear $[(A\text{-}\alpha\text{-}SiW_9O_{34})_2Co_8(OH)_6(H_2O)_2(CO_3)_3]^{16-}$ and $[Cu^{II}_8(L)_4(H_2O)_2(B\text{-}\alpha\text{-}XW_9O_{34})_2]^{4-}$ (X = Si^{IV}, Ge^{IV}; L = en, dap),[10a–d] nonanuclear $[(A\text{-}\alpha\text{-}SiW_9O_{34})_2Ni_9(OH)_6(H_2O)_6(CO_3)_3]^{14-}$ and $[H_4\{Cu^{II}_9As^{III}_6O_{15}(H_2O)_6\}(\alpha\text{-}As^{III}W_9O_{33})_2]^{8-}$,[11a,b] as well as two dodecanuclear $\{[Mn^{IV}_2Mn^{III}_6Mn^{II}_4(\mu_3\text{-}O)_6(\mu\text{-}OH)_4(H_2O)_2(CO_3)_6]\text{-}[B\text{-}\beta\text{-}SiW_6O_{26}]_2\}^{18-}$,[12] and $[\{Cu^{I}_2(2,2'\text{-}bpy)_2(4,4'\text{-}bpy)\}_2[Cu^{I}_2Cu^{II}_6(2,2'\text{-}bpy)_2(4,4'\text{-}bpy)_2(B\text{-}\alpha\text{-}GeW_9O_{34})_2\}]^{2-}$ complexes.[10b] Recently, a three-winged-shaped tetradeca-Fe^{III}-sandwiched nanocluster $[H_3Rb_3Fe_{14}(OH)_{12}(PO_4)_6(B\text{-}\alpha\text{-}PW_9O_{34})_2]\cdot 21H_2O$ with six phosphate linkers was discovered during the course of constructing much higher nuclear STMSP species.[13] Obviously, extraneous "stabilizers" such as small organic ligands (bpy, en, and dap) or inorganic anions (CO_3^{3-}, PO_4^{3-}, and $As_2O_5^{4-}$) have been employed, which reveal that these flexible "stabilizers" as structure-stabilizing agents (SSAs) can capture *in situ* generated high-nuclear TM aggregates derived from the inductive effect of lacunary POM fragments and the chelating coordination function of flexible "stabilizers" and effectively eliminate the synthetic obstacles in constructing higher nuclear STMSP species. Furthermore, the utilization of small inorganic or organic anionic ligands in the TM–POM system can facilitate the increase of the number of TM cores through increasing the negative charges of the desired compounds, accomplish unprecedented higher nuclear STMSP assemblies and extend structures from discrete molecules to 1-D chains, 2-D sheets and even 3-D frameworks. Nevertheless, the utilized organic addenda in the reported higher nuclear STMSPs are neutral aliphatic or aromatic amines. In contrast, there is still no report on the higher nuclear STMSPs by implanting polycarboxylate ingredients to increase the number

of TM cores, in which polycarboxylate groups simultaneously serve as connectors and extend the structure into a 1-D chain alignment, which is of great interest and provides excellent opportunities.

As an important subfamily of POMs, on the one hand, tungstoantimonates (TAs) have held the crucial position in the past several decades owing to their specific structural characteristics, especially the stereoactive lone-electron pair effect of the Sb^{III} heteroatom,[14] and the previously reported M-substituted TAs are dominated by the Krebs-type di-M-substituted polyanions $[Sb_2W_{20}M_2O_{70}(H_2O)_6]^{n-}$ (M = Fe^{III}, Co^{II}, Mn^{II}, Ni^{II}, Cu^{II}, Zn^{II}) and tetra-M substituted polyanions $[M_4(H_2O)_{10}(B\text{-}\beta\text{-}SbW_9O_{33})_2]^{6-}$ (M = Fe^{III}, Al^{III}),[6g,15] and their organic and organometallic derivatives.[5o,6r,16] The past decade has witnessed a great boost in the realm of TA-based TMSPs accompanied by the discovery of the purely inorganic Mn^{II}_6-hexagon TA $[(MnCl)_6(SbW_9O_{33})_2]^{12-}$ [8k] and the Fe^{III}_{11}-containing hexameric TA $[Fe_{11}(H_2O)_{14}(OH)_2(W_3O_{10})_2(\alpha\text{-}SbW_9O_{33})_6]^{27-}$,[17a] and the inorganic–organic hybrid 2,3-pyzdc-bridging TA $[(2,3\text{-pyzdc})_2\{NaNi_2(H_2O)_4\text{-}Sb_2W_{20}O_{70}\}_2]^{22-}$,[17b] the Ale-functionalized TA $[\{(SbW_9O_{33})_2Cu_3(H_2O)_{2.5}Cl_{0.5}\}_2\{Cu_6(Ale)_4(H_2O)_4\}_3]^{37-}$,[17c] and the homochiral macroanion $\{CoSb_6O_4(H_2O)_3[Co(hmta)SbW_8O_{31}]_3\}^{15-}$.[17d] A mixed-metal TA cluster $[H_{16}\{[Mn(OH_2)]_2W_7O_{32}\}\{Ag_4O_3[Mn(OH_2)]_2\}\text{-}(SbW_9O_{33})]^{9-}$ was also discovered recently.[17e] The recent progress in main-group metal or lanthanide substituted TAs is presented in the ESI.† These findings indicate that lacunary TA units can be modified artificially and have great potential to construct higher nuclear TM-substituted TAs.

On the other hand, among TMSPs, Mn-substituted POMs are a flourishing and burgeoning research theme due to their excellent magnetic merits. Hitherto, a handful of Mn-substituted-POM SMMs with $\{Mn^{III}_4Mn^{II}_2\}$, $\{Mn^{IV}Mn^{III}_6\}$, $\{Mn^{IV}Mn^{III}_3\}$, $\{Mn^{IV}_2Mn^{III}_6Mn^{II}_4\}$ and $\{Mn^{III}_4Mn^{II}_2O_4(H_2O)_{4-n}(L)_n\}$ (L = ethylenediamine, piperazine) groups that contain mixed-valence Mn–O cubane clusters possessing large uniaxial anisotropy induced by Jahn–Teller-elongated Mn^{III} centers have been successively reported,[8i,l,12,18] and good knowledge of SMM behaviors has also been gained. However, the continuous exploration of new architectures with unusual magnetic phenomena is a challenging task. Bearing these in mind, we have conducted research on the $[B\text{-}\alpha\text{-}SbW_9O_{33}]^{9-}/Mn^{2+}$ system in the presence of functional oxalic acid based on the following considerations: (a) besides the easy accessibility of the trilacunary TA precursor, the stereochemical influence of the lone-electron pair located in the trigonal pyramidal $\{SbO_3\}$ group can guarantee the existence of lacunary POM skeletons rather than saturated POM fragments in the process of reaction, facilitating the direct insertion of many more TM ions into the defect positions; (b) the functionality-carrying Mn^{2+} cation is chosen for its flexible and abundant coordination modes and the success in the assembly of extraordinary structural topologies with unexpected magnetic properties; (c) the versatile binding modes and configurations of oxalic acid can largely favor the construction of higher nuclear TM-substituted TAs with a great possibility of constructing extended architectures through linking metal centers, in the meantime, oxalic acid is a good electron transfer ligand that can improve the magnetic exchange interactions between metal centers by simultaneously offering the super-exchange pathway of σ and π electronic coupling; (d) the weak acidic or neutral aqueous environment is beneficial for the deprotonation of oxalic acid and increases the negative charge of the reaction system so as to induce the aggregation of more TM ions in the products. Thus, we successfully prepared a novel inorganic–organic hybrid 1-D sinusoidal chain nona-Mn^{II} sandwiched tungstoantimonate $Na_2H_4\{[Mn(H_2O)_3]_3[Mn(H_2O)_2]_2[Mn(H_2O)]\text{-}[Mn(C_2O_4)]_3[B\text{-}\alpha\text{-}SbW_9O_{33}]_2\}\cdot 31H_2O$ (**1**) (Scheme 1), which was structurally characterized by elemental analysis, IR spectroscopy, single-crystal X-ray diffraction, powder X-ray diffraction and thermal analyses. The results of magnetic studies show that the rare long-range ferromagnetic ordering and spin glass behavior coexist in **1**. It should be noted that **1** represents the first 1-D chain polyoxotungstate constructed from the nona-Mn^{II}-sandwiched TA units and double Mn^{II}–C_2O_4 linkages exhibiting the coexistence of long-range ordering and spin glass characteristics.

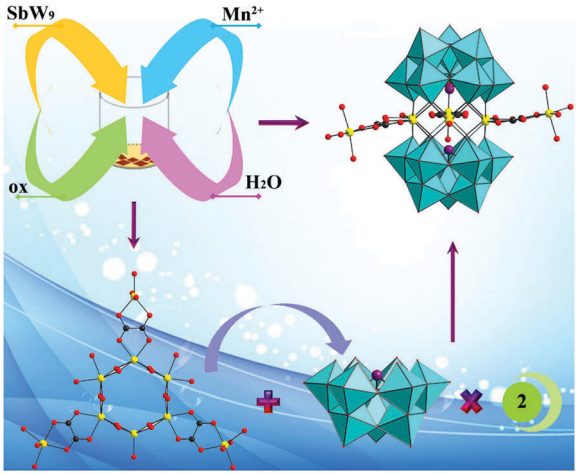

Scheme 1 The schematic synthetic process of **1**.

Experimental

Materials and physical measurements

The lacunary precursor $Na_9[B\text{-}\alpha\text{-}SbW_9O_{33}]\cdot 19.5H_2O$ was synthesized according to the literature method[19] and characterized by IR spectroscopy. All other reagents were obtained commercially and used without further purification. The C, H and N elemental analyses were carried out on a Perkin-Elmer 240C elemental analyzer. Inductively coupled plasma atomic emission spectrometry (ICP-AES) analyses were conducted on a Perkin-Elmer Optima 2000 ICP-AES spectrometer. IR spectra were recorded on a Nicolet 170 SXFT-IR spectrophotometer (using KBr pellets) in the range of 4000–400 cm^{-1}. Powder X-ray diffraction (PXRD) spectra were recorded on a Bruker D8 ADVANCE instrument with Cu Kα radiation (λ = 1.54056 Å) in the angular range 2θ = 5–40° at 293 K. UV spectra were recorded on a HITACHI U-4100 UV-Vis-NIR spectrometer. Thermogravimetric (TG), derivative thermogravimetric (DTG) and differential thermal analyses (DTA) were carried out on the crystal sample of **1** using a Mettler-Toledo TGA/SDTA 851^e

instrument with a heating rate of 10 °C min^{-1} from 25 °C to 800 °C under a flowing N_2 atmosphere. X-ray photoelectron spectra (XPS) were recorded with an Axis Ultra X-ray photoelectron spectrometer. The field dependence of magnetization at different temperatures and variable temperature (1.8–300 K) magnetic susceptibility measurements were performed with a Quantum Design MPMS XL-7 magnetometer and the magnetic data were corrected from diamagnetic contributions estimated from Pascal's constants.

Preparation of $Na_2H_4\{[Mn(H_2O)_3]_3[Mn(H_2O)_2]_2[Mn(H_2O)][Mn(C_2O_4)]_3[B\text{-}\alpha\text{-}SbW_9O_{33}]_2\}\cdot 31H_2O$ (1)

$Na_9[B\text{-}\alpha\text{-}SbW_9O_{33}]\cdot 19.5H_2O$ (2.500 g, 0.873 mmol), $MnCl_2\cdot 4H_2O$ (1.500 g, 7.579 mmol) and oxalic acid (0.080 g, 0.635 mmol) were dissolved in 20 mL of distilled water under continuous stirring. The pH was adjusted to 6.3 by 2 mol L^{-1} NaOH aqueous solution. Followed by another 30 min of stirring, the resulting solution was heated at 90 °C for 1 h, cooled to room temperature and filtered. After several days, light yellow microcrystals appeared and were filtered out. Upon continuous evaporation at room temperature, red rhombus desired crystals were harvested from the filtrate in about one month. Yield: 21% (based on oxalic acid). Elemental analysis calcd (%) for **1**: C, 1.15; H, 1.52; Na, 0.74; Mn, 7.94; Sb, 3.91; W, 53.13; found (%): C, 1.32; H, 1.64; Na, 0.65; Mn, 7.79; Sb, 3.96; W, 52.88. IR (KBr pellet, cm^{-1}): 3402 (s), 1647 (s), 1317 (m), 944 (s), 868 (s), 825 (s), 726 (s), 474 (w).

X-ray crystallography

A good-quality crystal of **1** was picked up from the mother liquor and mounted on fiber glass. Diffraction intensity data were collected at 296 K on a Bruker Apex-II CCD diffractometer equipped with graphite-monochromated Mo Kα radiation (λ = 0.71073 Å). Routine Lorentz and polarization corrections were employed and a multi-scan absorption correction was utilized with the SADABS program.[20] Direct methods were used to solve the structure and locate the heavy atoms using the SHELXTL-97 program.[21] The remaining atoms were found from successive full-matrix least-squares refinements on F^2 and Fourier syntheses. No hydrogen atoms associated with water molecules were located from the difference Fourier map. All non-hydrogen atoms were refined anisotropically except for some oxygen atoms and water molecules. Crystallographic data and structural refinement parameters for **1** are summarized in Table 1. CCDC 1513036 (**1**).

Table 1 Crystallographic data and structure refinements for **1**

	1
Empirical formula	$C_6H_{94}Mn_9Na_2O_{123}Sb_2W_{18}$
Formula weight	6228.05
Crystal system	Monoclinic
Space group	*C*2/*c*
a, Å	18.061(4)
b, Å	27.381(6)
c, Å	23.825(5)
α, deg	90
β, deg	106.140(4)
γ, deg	90
V, $Å^{-3}$	11318(4)
Z	4
μ, mm^{-1}	19.777
F(000)	11180
T, K	296(2)
Limiting indices	$-16 \le h \le 21$ $-31 \le k \le 32$ $-27 \le l \le 28$
No. of reflections collected	28 233
No. of independent reflections	9863
R_{int}	0.0621
Data/restrains/parameters	9863/12/658
GOF on F^2	1.021
Final *R* indices [$I > 2\sigma(I)$]	R_1 = 0.0459 wR_2 = 0.1148
R indices (all data)	R_1 = 0.0727 wR_2 = 0.1243
Largest diff. peak and hole, e $Å^{-3}$	2.774, −2.631

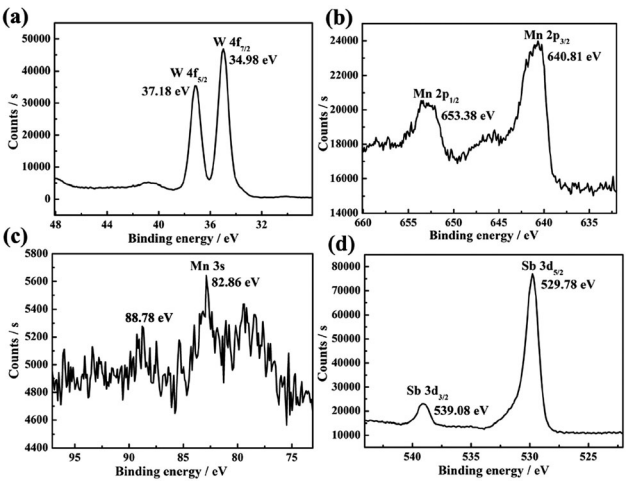

Fig. 2 XPS spectra of **1** for (a) W $4f_{5/2}$ and W $4f_{7/2}$; (b) Mn $2p_{1/2}$ and Mn $2p_{3/2}$; (c) Mn 3s; (d) Sb $3d_{3/2}$ and Sb $3d_{5/2}$.

Results and discussion

Structural description

Bond valence sum (BVS) calculations[22] manifest that the oxidation states of all W, Sb and Mn centers are assigned to +6, +3 and +2, respectively (Table S1, ESI†). Specifically speaking, the BVS values of the W1, W2, W3, W4, W5, W6, W7, W8, W9, Mn1, Mn2, Mn3, Mn4, Mn5 and Sb1 centers are 5.96, 6.25, 6.02, 6.04, 6.01, 6.05, 6.11, 6.11, 6.09, 2.07, 2.00, 2.02, 1.89, 2.10 and 2.88, respectively.

The XPS spectra of **1** were also recorded to further consolidate the chemical valences of W, Sb and Mn atoms (Fig. 2). The two overlapped strong peaks with binding energies (BEs) of 37.18 and 34.98 eV in the XPS pattern are ascribed to W^{VI} ($4f_{5/2}$) and W^{VI} ($4f_{7/2}$) (Fig. 2a). These observed values are basically in agreement with the previously reported values of the W^{VI} components.[23] The Mn 2p spectrum splits into two peaks of Mn $2p_{1/2}$ and Mn $2p_{3/2}$ owing to the spin–orbit doublet, and their binding energies are, respectively, located at 653.38 and 640.81 eV (Fig. 2b), suggesting a uniform +2 oxidation state of all the Mn centers, which well coincides with the values observed

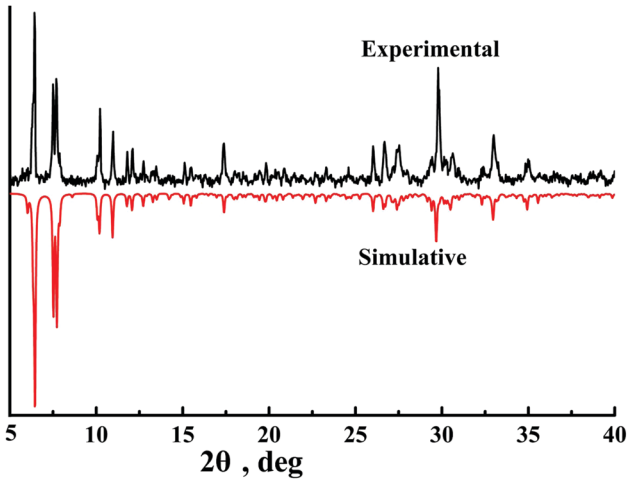

Fig. 3 Comparison of the PXRD pattern of **1** and its single-crystal XRD pattern.

in the pure MnO.[24] Additionally, the extent of Mn 3s multiplet splitting measured simultaneously offers additional insight into the Mn chemical states.[24a] In the case of **1**, the Mn 3s multiplet splitting value of 5.92 eV also suggests the +2 chemical state of the Mn centers (Fig. 2c). Besides, two apparent signals appearing at 539.08 and 529.78 eV correspond to the Sb $3d_{3/2}$ and Sb $3d_{5/2}$ of the Sb^{III} center (Fig. 2d), and the Sb $3d_{3/2}$ and Sb $3d_{5/2}$ BE values in **1** are consistent with those [539.13 (Sb $3d_{3/2}$) and 529.77 eV (Sb $3d_{5/2}$)] observed in the pure Sb_2O_3 crystal.[25] These results agree well with the structural analysis. Furthermore, the phase purity of **1** was confirmed by the good consistency of its experimental PXRD pattern with that calculated from the single-crystal X-ray diffraction (Fig. 3) and the intensity discrepancy between the experimental and simulated PXRD patterns may be resulted from the preferred orientation variation of the powder sample.

Single-crystal structural analysis reveals that **1** crystallizes in the monoclinic space group *C*2/*c*. The molecular structural unit of **1** (Fig. S1, ESI†) consists of an unprecedented nona-Mn^{II} substituted sandwich-type polyanion $\{[Mn(H_2O)_3]_3[Mn(H_2O)_2]_2[Mn(H_2O)][Mn(C_2O_4)]_3[B\text{-}\alpha\text{-}SbW_9O_{33}]_2\}^{6-}$ (Fig. 4a and h), in which the nona-Mn^{II} $\{[Mn(H_2O)_3]_3[Mn(H_2O)_2]_2[Mn(H_2O)][Mn(C_2O_4)]_3\}^{12+}$ (Mn_9) hybrid cluster core is encapsulated by two symmetrical trivacant Keggin $[B\text{-}\alpha\text{-}SbW_9O_{33}]^{9-}$ TA fragments, giving rise to the beautiful sandwich assembly. Upon close inspection of the particular Mn_9 cluster core (Fig. 4b), it is remarkably interesting to find that this unusual nona-Mn^{II} cluster core can be considered as a hexagonal $\{Mn_6(H_2O)_5(C_2O_4)_3\}^{6+}$ (Mn_6) cluster with the incorporation of three alternating pedant $[Mn(H_2O)_3]^{2+}$ groups. The organic–inorganic hybrid hexagonal $\{Mn_6\}$ cluster is constructed from five $\{MnO_6\}$ octahedra and one $\{MnO_5\}$ square pyramid through edge-sharing mode, which is completely distinct from the inorganic hexagonal $[Mn_6Cl_6]^{6+}$ cluster in $[(MnCl)_6(SbW_9O_{33})_2]^{12-}$ that is formed by six $\{MnO_4Cl\}$ square pyramids through the edge-sharing mode.[8k] More appealingly, there are six crystallographically unique Mn^{2+} ions ($Mn1^{2+}$–$Mn6^{2+}$) in the nona-Mn^{II} cluster core, which simultaneously display four kinds of coordination

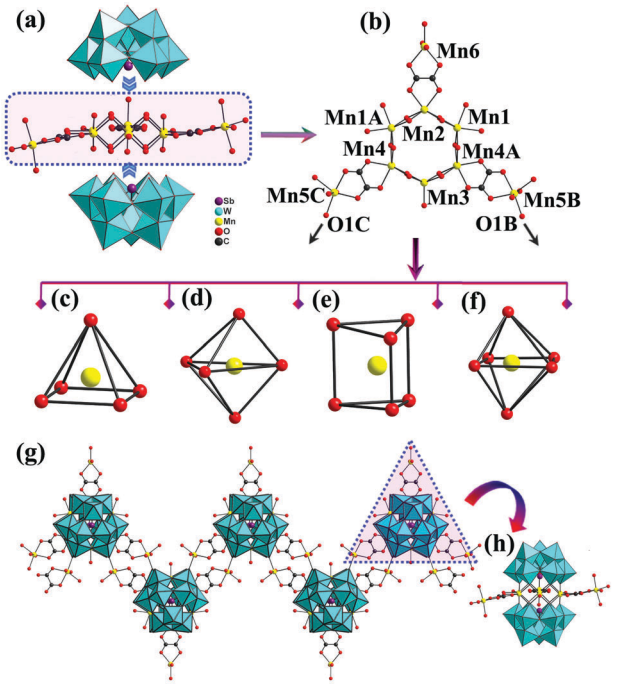

Fig. 4 (a) and (h) Combined polyhedral and ball-and-stick views of the molecular structural unit of **1**; (b) the nona-nuclear $\{Mn_9\}$ hybrid cluster in **1**; (c) the hexa-coordinate triangular prism geometry of $Mn1^{2+}$, $Mn2^{2+}$ and $Mn4^{2+}$ cations; (d) the penta-coordinate square pyramid configuration of the $Mn3^{2+}$ cation; (e) the hexa-coordinate distorted octahedral geometry of the $Mn5^{2+}$ cation; (f) the penta-coordinate trigonal bipyramid geometry of the $Mn6^{2+}$ cation; (g) the 1-D sinusoidal chain in **1**. The atoms with the suffix A are generated by the symmetry operation, where *A*: $1-x, y, 0.5-z$, *B*: $1-x, -1-y, 1-z$, and *C*: $x, -1-y, -0.5+z$.

geometries (Fig. 4c–f and Fig. S2, ESI†). Such a phenomenon is rarely seen in POM chemistry. Specifically, the $Mn1^{2+}$, $Mn2^{2+}$ and $Mn4^{2+}$ cations reside in the hexa-coordinate triangular prism geometries defined by four μ_3-O atoms from two $[B\text{-}\alpha\text{-}SbW_9O_{33}]^{9-}$ fragments [Mn–O: 2.149(11)–2.224(9) Å] and two O atoms from two coordinated water molecules [Mn–O: 2.204(11)–2.206(10) Å] or one oxalate anion [Mn–O: 2.184(10)–2.238(10) Å] (Fig. 4c and Fig. S2a–c, ESI†). The $Mn3^{2+}$ cation employs a penta-coordinate square pyramid configuration, in which the basal positions are occupied by four O atoms from two $[B\text{-}\alpha\text{-}SbW_9O_{33}]^{9-}$ fragments [Mn–O: 2.120(10)–2.158(9) Å] and the axial position is occupied by an aqueous ligand [Mn–O: 2.10(3) Å] (Fig. 4d and Fig. S2d, ESI†). The $Mn5^{2+}$ cation is embedded in a hexa-coordinate distorted octahedral geometry where three water ligands and one O atom from one oxalate anion stand on the equatorial plane [Mn–O: 2.138(15)–2.220(13) Å] and one terminal O atom from a $[B\text{-}\alpha\text{-}SbW_9O_{33}]^{9-}$ fragment and one O atom from an oxalate anion are located at two polar sites [Mn–O: 2.156(9)–2.195(11) Å] (Fig. 4e and Fig. S2e, ESI†). The $Mn6^{2+}$ cation adopts the penta-coordinate trigonal bipyramid environment, in which one aqueous ligand and two O atoms from one oxalate anion constitute the triangular plane [Mn–O: 2.21(8)–2.192(18) Å] and two aqueous ligands inhabit two vertices [Mn–O: 2.174(17) Å] (Fig. 4f and Fig. S2f, ESI†). These observations further demonstrate that the functionality-carrying Mn^{2+} cations can utilize

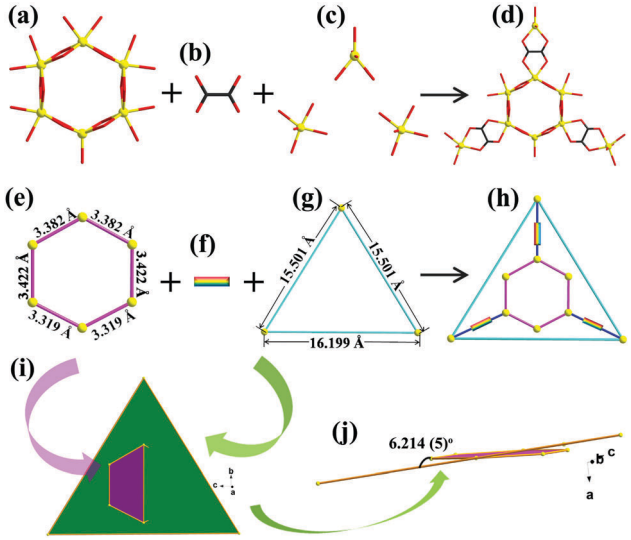

Fig. 5 (a) View of the internal hexagonal $\{Mn_6\}$ core; (b) view of the oxalate ligand; (c) view of three external Mn^{2+} cations distributed in an equicrural triangle fashion; (d) view of the $\{Mn_9\}$ cluster; (e) the simplified $\{Mn_6\}$ core with neighboring Mn···Mn distances of 3.321–3.420 Å; (f) the simplified oxalate bridge; (g) the simplified $\{Mn_3\}$ plane defined by three external Mn^{2+} cations with Mn···Mn distances ranging from 15.498 to 16.195 Å; (h) the simplified $\{Mn_9\}$ cluster; (i) and (j) the $\{Mn_6\}$ plane and the $\{Mn_3\}$ plane are almost coplanar with a small dihedral angle of about 6.2°.

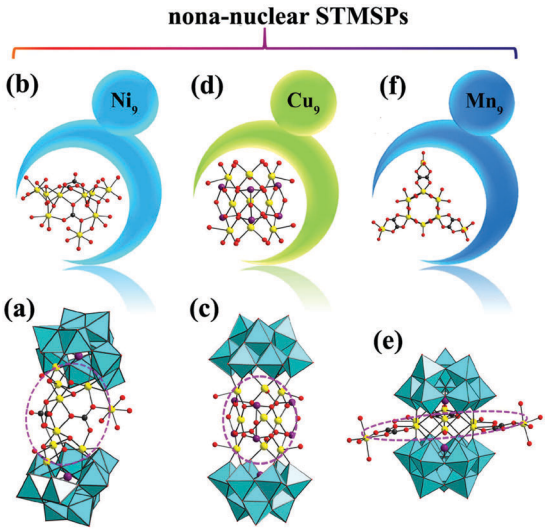

Fig. 6 (a) View of $[(A\text{-}\alpha\text{-}SiW_9O_{34})_2Ni_9(OH)_6(H_2O)_6(CO_3)_3]^{14-}$. (b) View of the $[Ni_9(OH)_6(H_2O)_6(CO_3)_3]^{6+}$ (Ni_9) core. (c) View of $[H_4\{Cu^{II}_9As^{III}_6O_{15}(H_2O)_6\}(\alpha\text{-}As^{III}W_9O_{33})_2]^{8-}$. (d) View of the $[Cu^{II}_9As^{III}_6O_{15}(H_2O)_6]^{6+}$ (Cu_9) core. (e) View of **1**. (f) View of the $\{Mn_9\}$ core in **1**.

the flexible and abundant coordination modes in the construction of the structure.

As anticipated, oxalate ligands participate in the coordination of the $\{Mn_9\}$ cluster core. The distribution motif of nine Mn^{2+} cations in **1** can be described as follows (Fig. 5): the internal six Mn^{2+} ions are interconnected *via* double μ_2-O atoms making a planar hexagonal $\{Mn_6\}$ core with neighboring Mn···Mn distances of 3.319–3.422 Å (Fig. 5a and e), and another three external Mn^{2+} cations (Fig. 5c and g) (Mn_3) grafting to the internal $\{Mn_6\}$ core through three oxalate ligands (Fig. 5b and f) are located at three vertices of the equicrural triangle with the Mn···Mn distances ranging from 15.501 to 16.199 Å, giving rise to the unseen nona-Mn^{II} cluster functionalized by oxalate ligands (Fig. 5d and h). What is more, the inner hexagonal $\{Mn_6\}$ plane and three external Mn^{2+} cations are approximately coplanar with a small dihedral angle of about 6.2° (Fig. 5i and j). The phenomenon that three oxalate ligands superseding six water molecules participate in the coordination to three Mn^{2+} cations situated at the alternating sites of a $\{Mn_6\}$ ring is for the first time encountered in the chemistry of TMSPs, although the substitution of three water molecules by three acetate ligands was previously observed in $[Na_3(H_2O)_6Mn_3(\mu\text{-}OAc)_2(B\text{-}\alpha\text{-}SbW_9O_{33})_2]^{11-}$.[5j]

Dramatically different from another two nona-nuclear STMSPs, $[(A\text{-}\alpha\text{-}SiW_9O_{34})_2Ni_9(OH)_6(H_2O)_6(CO_3)_3]^{14-}$ (Fig. 6a)[11a] comprising double-cube subunits linked by three carbonato ligands capping the ninth Ni^{II} atom (Fig. 6b) and $[H_4\{Cu_9As_6O_{15}(H_2O)_6\}(\alpha\text{-}AsW_9O_{33})_2]^{8-}$ (Fig. 6c) containing a cylindrical $\{Cu^{II}_9As^{III}_6O_{15}(H_2O)_6\}^{6+}$ core[11b] (Fig. 6d), the $\{Mn_9\}$ motif is innovative and unparalleled and contains a hexagonal $\{Mn_6\}$ ring surrounded by a peripheral $\{Mn_3\}$ triangle through three inner oxalate bridges, leading to an approximately coplanar $\{Mn_9\}$ cluster; although they all obtain high-nuclear STMSPs in the presence of SSAs, the former two are discrete architectures whilst **1** shows an interesting 1-D chainlike arrangement, which makes **1** outperform many reported STMSPs. Besides, in the case of the $\{Mn_6\}$ ring, in particular for a hexagon, it is reminiscent of the species $[(MnCl)_6(SbW_9O_{33})_2]^{12-}$ (**2**) that was addressed by Yamase *et al.*,[8k] in which each Mn^{2+} cation in the hexagonal ring is bound to an external Cl^- anion. Nonetheless, there are four obvious discrepancies between them: (a) oxalate ligands were successfully introduced in **1** (Fig. 6e), which not only act as SSAs but also serve as bridging agents through the coordination of carboxylate O atoms, and these effectively increase the Mn^{2+} nuclearity and extend the isolated unit to a 1-D chain, whereas **2** exhibits a discrete hexa-Mn^{II} sandwich structure due to the absence of any SSA; (b) **1** encompasses six crystallographically unique Mn^{2+} cations while **2** only consists of one crystallographically unique Mn^{2+} cation; (c) Mn^{2+} cations in **1** show four kinds of coordination geometries with the coordination numbers ranging from 5 to 6, but in **2**, only a penta-coordinate Mn^{2+} motif is observed; (d) the coordination atoms in **1** are unitary O atoms from the $[B\text{-}\alpha\text{-}SbW_9O_{33}]^{9-}$ subunits, carboxylate O atoms and water molecules whereas the coordination spheres in **2** involve the O atoms from the $[B\text{-}\alpha\text{-}SbW_9O_{33}]^{9-}$ fragments and Cl^- anions. In addition, the $\{Mn_9\}$ core in **1** (Fig. 6f) can be deemed as a structure with the partially coordinated water molecules of the hexagonal $\{Mn_6\}$ ring superseded by Mn–C_2O_4 complexes. Actually, the POMs that coordinate aqueous molecules bound to TM atoms are active enough to be replaced partially or completely by N/O-containing organic ligands, providing the possibility of constructing high-nuclear inorganic–organic hybrid TMSPs. This research concept has been verified by several groups. For instance, Zhao and Yang reported a series of STMSPs containing double-cubane $\{Mn^{III}_4Mn^{II}_2O_4(H_2O)_4\}$ cores with water ligands

substituted by two or four organic ligands.[8l] Zhou's group synthesized three novel TM_6-sandwiched tungstoarsenates with the hexagonal metallocycles fully adorned by imidazole ornaments.[8o] On the basis of a similar strategy, Yang's group also communicated a class of octa-Cu-based STMSPs decorated by dap, en or bpy, as well as a dodeca-Cu aggregate constructed from the octa-Cu-based STMSPs and two Cu^{I}-complexes ($[Cu^{I}_2(2,2'\text{-bpy})_2(4,4'\text{-bpy})]$) through 4,4′-bpy linkers.[10b] In terms of this methodology, much more work is still desired to acquire abundant inorganic–organic hybrid STMSPs *via* carefully tuning the reaction conditions.

The most remarkable structural characteristic of **1** is that adjacent $\{[Mn(H_2O)_3]_3[Mn(H_2O)_2]_2[Mn(H_2O)][Mn(C_2O_4)]_3[B\text{-}\alpha\text{-}SbW_9O_{33}]_2\}^{6-}$ units are fused together by the double Mn–C_2O_4 linkers, giving birth to the beauteous 1-D sinusoidal chain (Fig. 4g), in which $[Mn5(C_2O_4)(H_2O)_3]$ and $[Mn5A(C_2O_4)(H_2O)_3]$ groups work as connectors favoring the formation of the 1-D chain and the $[Mn6(C_2O_4)(H_2O)_3]$ groups function as pendants supporting both sides of the 1-D chain. Another linear chain with a double-bridging mode has been encountered in the Cu_6-based TMSP $[Cu_6(\mu_3\text{-}OH)_3(en)_3(H_2O)_3(B\text{-}\alpha\text{-}PW_9O_{34})]\cdot 4H_2O$ reported by Yang's lab,[26] but different from **1**, this 1-D chain is based on the $[Cu_6(\mu_3\text{-}OH)_3(en)_3(H_2O)_3(B\text{-}\alpha\text{-}PW_9O_{34})]$ units through terminal O atoms from the $[B\text{-}\alpha\text{-}PW_9O_{34}]^{9-}$ fragments. As far as we are aware, **1** represents the first example of an endless sinusoidal chain assembled from nona-Mn^{II}-sandwiched TA units and double Mn–C_2O_4 linkages. Weak intermolecular interactions play an important role in controlling the packing or assembly of supramolecular architectures. In **1**, adjacent chains are interconnected *via* feeble π···π stacking existing between contiguous oxalate ligands with a distance of 6.57 Å (Fig. S3, ESI†), generating a 3-D stacking framework that is piled up regularly in the –AAA– mode (Fig. 7a and Fig. S4a, ESI†). These sinusoidal chains are distributed parallelly in the *a*-axis forming a layer across the *bc* plane with the interchain distance of 16.40 Å (Fig. 7b), and in the *c*-axis forming a layer across the *ab* plane with the interchain distance of 13.10 Å (Fig. 7b and Fig. S4b, ESI†). Though the π···π stacking and interchain interactions are weak, they may contribute to the magnetic exchange and lead to long-range magnetic ordering.

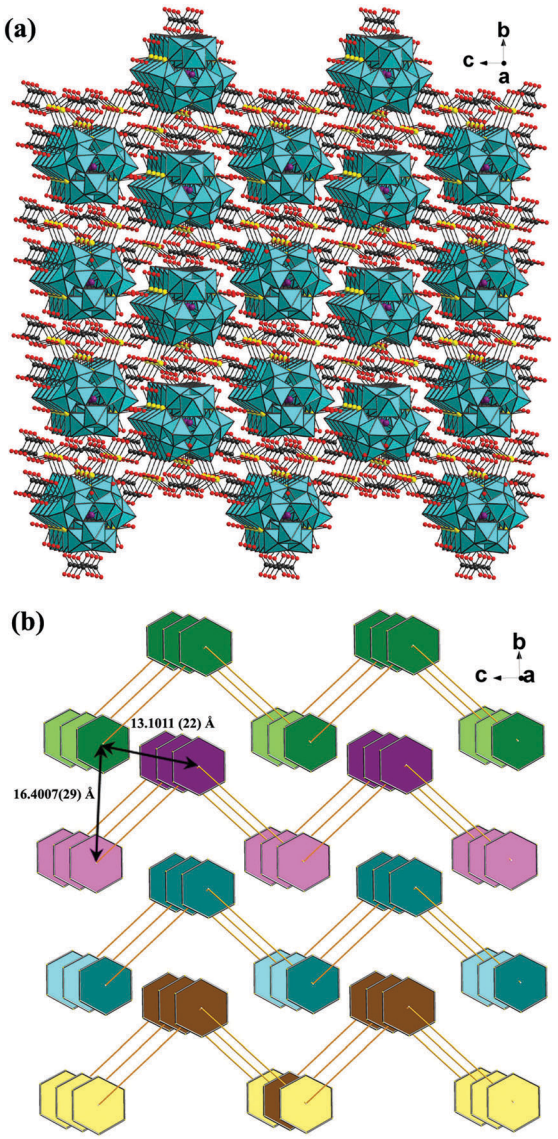

Fig. 7 (a) The 3-D packing architecture of **1** viewed along the *a*-axis; (b) the simplified 3-D packing mode of **1** viewed along the *a*-axis.

IR spectra

The IR spectrum of **1** (Fig. 8a and Fig. S5, ESI†) was recorded on a Nicolet 170 SXFT-IR spectrophotometer using KBr pellets in the range of 4000–400 cm^{-1}, which exhibits four characteristic vibration bands of ν(Sb–O_a), terminal ν(W–O_t), corner-sharing ν(W–O_b), and edge-sharing ν(W–O_c) derived from the trilacunary Keggin $[B\text{-}\alpha\text{-}SbW_9O_{33}]^{9-}$ skeleton, appearing at 726, 944, 825 and 687 cm^{-1}, respectively. It should be noted that largish shifts of the ν(W–O) and ν(Sb–O) characteristic patterns are observed in comparison with the precursor $[B\text{-}\alpha\text{-}SbW_9O_{33}]^{9-}$ (Fig. 8b and Fig. S6, ESI†) [767, 920, 890 and 715 cm^{-1} for ν(Sb–O_a), ν(W–O_t), ν(W–O_b) and ν(W–O_c)],[19] which are probably attributable to the incorporation of the $\{Mn_9\}$ cluster into the defect sites of two $[B\text{-}\alpha\text{-}SbW_9O_{33}]^{9-}$ segments leading to the distortion of the $[B\text{-}\alpha\text{-}SbW_9O_{33}]^{9-}$ skeleton. However, the IR spectrum of **1** is somewhat similar to that of $[(MnCl)_6(SbW_9O_{33})_2]^{12-}$ (725, 942, 813 and 683 cm^{-1}),[8k] indicating that the hexagonal Mn_6-substituted TA subunit still remains in **1**. The slight movement of the characteristic peaks may be relevant to the grafting of metal–organic complexes onto the $\{Mn_6\}$ ring in the central belt. In the high-wavenumber region ($\nu > 1000$ cm^{-1}), two intense absorption peaks appearing at 3402 cm^{-1} and 1647 cm^{-1} are assigned to the stretching and bending vibrations of ν(O–H) groups, reflecting the presence of coordinated and lattice water molecules. Actually, the asymmetric stretching vibration of the carboxylate group of the oxalate ligand is overlapped by the intense bending vibration bands of ν(O–H) groups of water ligands. In the IR spectrum of **1**, the band at 1647 cm^{-1} is also indicative of the asymmetric stretching vibration of the carboxylic group [denoted as $\nu_{as}(CO_2^-)$] whilst the signal at 1362 cm^{-1} is ascribed to the symmetric stretching vibration of the carboxylic group [denoted as $\nu_s(CO_2^-)$]. In the IR spectrum of the free oxalic acid ligand (Fig. 8c and Fig. S7, ESI†), the $\nu_{as}(CO_2^-)$ and $\nu_s(CO_2^-)$

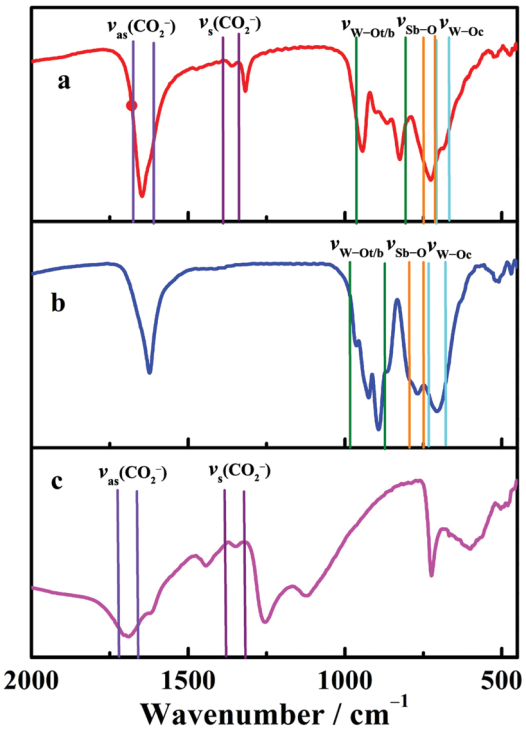

Fig. 8 Comparison of the IR spectra of **1** (a), $Na_9[B\text{-}\alpha\text{-}SbW_9O_{33}]\cdot 19.5H_2O$ (b) and oxalic acid (c) in the range of 2000–400 cm^{-1}.

stretching vibration bands appear at 1690 and 1348 cm^{-1}. In comparison with the IR spectrum of the free oxalic acid ligand, the $\nu_{as}(CO_2^-)$ and $\nu_s(CO_2^-)$ vibration bands of **1** are obviously shifted for 43 and 14 cm^{-1} as a consequence of covalent coordination of the oxalate ligands with Mn^{2+} cations.[27] In general, the separation ($\Delta\nu$) between $\nu_{as}(CO_2^-)$ and $\nu_s(CO_2^-)$ in the IR spectrum has been successfully utilized as a criterion to evaluate the bonding mode of the carboxylic groups.[28] If $\Delta\nu$ is larger than 200 cm^{-1}, carboxylic groups adopt the monodentate coordination mode; correspondingly, if $\Delta\nu$ is smaller than 200 cm^{-1}, carboxylic groups make use of the chelating coordination fashion.[28c] In the case of **1**, different from monodentate and chelating coordination modes, the much larger separation of 285 cm^{-1} interprets the bridging mode of the oxalate ligand. In summary, the results of IR spectroscopy are in good agreement with those of X-ray single-crystal structural analysis.

Magnetic properties

POM matrices with unique electronic and structural characteristics not only possess the ability to serve as inorganic ligands embedding exchange-coupled paramagnetic TM clusters but also show great potential as ideal magnetic insulation materials that may dilute the magnetic units and effectively shield the magnetic cores from interactions with other molecules. These POM frameworks offer a good opportunity to investigate magnetic exchange interactions within TM clusters encapsulated by POM matrices and study the electron delocalization effect in highly symmetrical clusters, as well as control the magnitude of magnetic couplings.[29] In this paper, a comprehensive study on the magnetic behaviors of **1** was carried out considering the presence of the well-isolated oxalate-functionalized $\{Mn_9\}$ core between two nonmagnetic TA fragments.

Magnetic susceptibility measurements of the crystalline sample of **1** were performed using a Quantum Design MPMS

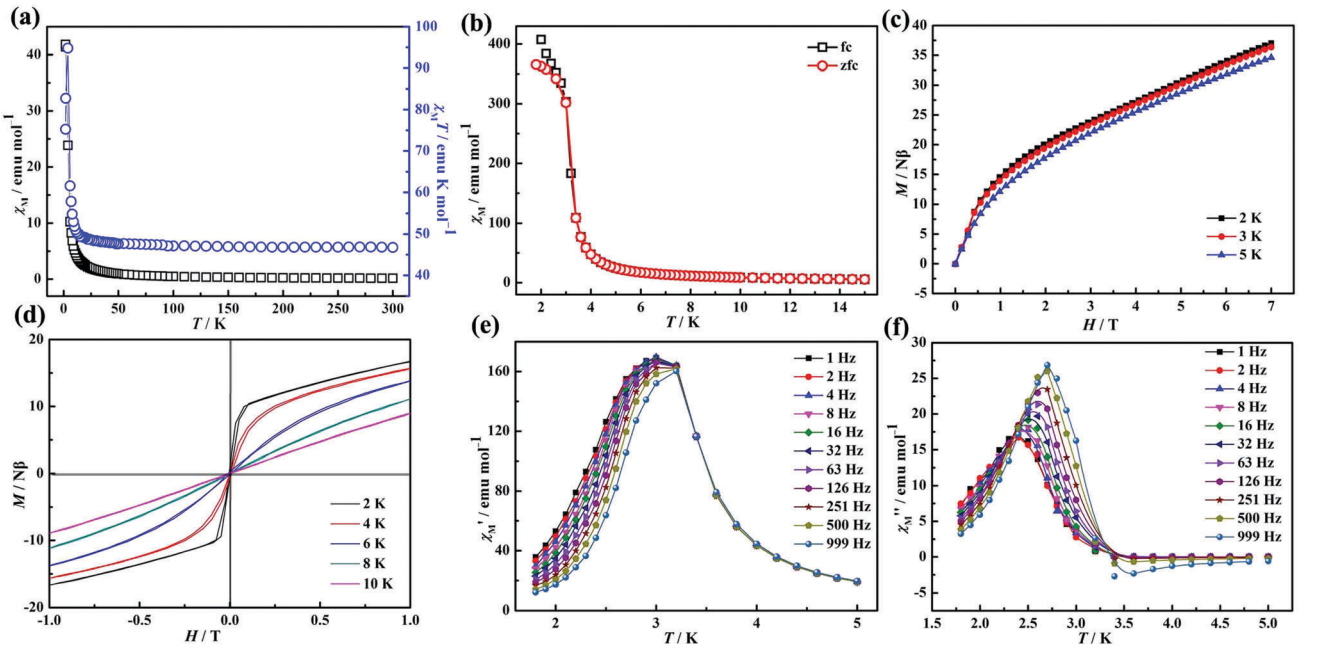

Fig. 9 (a) Temperature dependence of χ_M and $\chi_M T$ for **1** between 1.8 K and 300 K at 1000 Oe; (b) the plots of zero-field-cooling magnetization and field-cooled magnetization at 10 Oe; (c) field dependence of magnetization of **1** at various temperatures; (d) hysteresis loops for **1** measured at different temperatures at a sweeping rate of 500 Oe s^{-1}; (e) ac measurements of the in-phase (χ_M') for **1** under a zero static field; (f) ac measurements of the out-of-phase (χ_M'') for **1** under a zero static field.

XL 7 magnetometer from 1.8 K to 300 K under a 1000 Oe dc field. As shown in Fig. 9a, the χ_M slowly increases from 0.16 emu mol^{-1} at 300 K to 2.21 emu mol^{-1} at 22 K, and then exponentially to the maximum of 41.81 emu mol^{-1} at 1.8 K. The $\chi_M T$ value is 46.7 emu K mol^{-1} at 300 K, which is slightly higher than the spin-only value of 39.4 emu K mol^{-1} expected for nine uncoupled Mn(II) ions (S = 5/2, g = 2). Upon lowering the temperature, the $\chi_M T$ value increases moderately to 49.4 emu K mol^{-1} at 15 K and then abruptly reaches a maximum of 94.8 emu K mol^{-1} at 3.9 K. This behavior demonstrates the dominant ferromagnetic (FM) interactions within Mn^{2+} centers, which can be further consolidated by the apparently unsaturated magnetization value of 37.0 Nβ under a 7 T magnetic field. Eventually, the $\chi_M T$ value sharply drops to 75.3 emu K mol^{-1} at 1.8 K, which may be attributed to the occurrence of the zero-field splitting (ZFS) effect, the antiferromagnetic (AFM) interactions within Mn^{2+} centers and/or intermolecular interactions in **1**. Besides, according to the Curie–Weiss law, the linear fitting of the magnetic data of χ_M *vs.* T in the whole temperature range yields the positive Weiss temperature θ = 1.1 K and the Curie constant C = 46.6 emu K mol^{-1} (Fig. S8, ESI†), and the small positive θ value further corroborates the weak dominant FM interactions in **1**. In the structure of **1**, the nona-Mn^{II} $\{[Mn(H_2O)_3]_3[Mn(H_2O)_2]_2[Mn(H_2O)][Mn(C_2O_4)]_3\}^{12+}$ hybrid cluster is embraced by two symmetrical trivacant Keggin $[B\text{-}\alpha\text{-}SbW_9O_{33}]^{9-}$ fragments and the nona-Mn^{II} cluster can be viewed as a hexagonal hexa-Mn^{II} $\{Mn_6(H_2O)_5(C_2O_4)_3\}^{6+}$ cluster coordinated by three alternating pedant $[Mn(H_2O)_3]^{2+}$ groups *via* three oxalate ligands. On the basis of the previous reported documents,[30] it is clearly found that oxalate ligands always mediate the AFM interactions between Mn^{2+} centers. Thereby, it can be deduced that the magnetic couplings within $Mn2^{2+}\cdots Mn6^{6+}$, $Mn4^{2+}\cdots Mn5C^{6+}$, and $Mn4A^{2+}\cdots Mn5B^{6+}$ centers (Fig. 4b) are AFM interactions. However, dominant FM interactions occur in **1**, therefore, we can basically conclude that the predominant FM interactions of **1** principally stem from the FM contribution of the hexagonal $\{Mn_6(H_2O)_5(C_2O_4)_3\}^{6+}$ cluster. As a matter of fact, the FM interactions of the similar hexagonal hexa-Mn^{II} $[Mn_6Cl_6]^{6+}$ cluster in $[(MnCl)_6(SbW_9O_{33})_2]^{12-}$ were investigated by Yamase's group.[8k] So, FM and AFM interactions coexist in **1**. Furthermore, to determine the existence of the possible magnetic phase transition demonstrated by the hump of the $\chi_M T$ curve at around 3.9 K, zero-field-cooling (zfc) and field-cooled (fc) magnetization measurements were performed in the temperature region of 2–16 K under 10 Oe (Fig. 9b), which exhibit an abrupt increase below 4 K and have an evident divergence at around 3 K, implying the appearance of long-range FM ordering in **1**.[31a]

The field dependence of magnetization of **1** was performed at 2 K (Fig. S9, ESI†). As the field arises, the magnetization rapidly increases up to about 1 T, and then continually ascends to the maximum of 37.0 Nβ at 7 T, which is lower than the saturated value of 45 Nβ expected for nine Mn^{2+} ions (assuming g = 2). Besides, the field dependence of the magnetization has also been recorded up to 7 T between 2 and 5 K (Fig. 9c). The almost superposition of the isofield lines reveals the presence of the weak ZFS effect,[31b] which interprets that the sharp drop of the $\chi_M T$ value below 3.9 K is mainly attributed to the AFM interactions within Mn^{2+} centers and/or intermolecular interactions in **1**. Furthermore, the low-temperature hysteresis loops for **1** were recorded between 2 and 10 K within ±1 T at a sweeping rate of 500 Oe s^{-1} (Fig. 9d). At 2 K, the initial magnetization increases abruptly up to 10 Nβ at 0.08 T, and then increases linearly up to 1 T. Butterfly-shaped hysteresis loops could be clearly seen below 8 K and become apparent upon decreasing temperature, which all exhibit unsaturated magnetization. The behavior of the larger departure from the saturation of the field dependence of magnetization and the appearance of the hysteresis loops suggest a spin-canted weak ferromagnetic state in **1**,[31c] probably arising from the contribution of the FM $\{Mn_6(H_2O)_5(C_2O_4)_3\}^{6+}$ cluster. The canting angle α can be estimated from the equation $\sin(\alpha) = M_R/M_S$,[32] where M_R is the remnant magnetization and M_S is the saturated magnetization. A hysteresis loop with the coercive field (H_c) and the remnant magnetization (M_R) at 2 K of 4.3 Oe and 0.89 Nβ (Fig. S10, ESI†) was observed, thus giving the α value of about 1.1°. Additionally, the hysteresis loop becomes narrower and nearly ambiguous upon decreasing the field sweep rate to 100 Oe s^{-1} (Fig. S10–S12, ESI†), suggesting the possible quantum tunneling of the magnetization of **1**.

Alternating current (ac) magnetic susceptibility measurements of **1** were performed in the temperature range of 1.8–5 K under a zero static field oscillating at frequencies in the 1–999 Hz range. As revealed in Fig. 9e and f, both the in-phase (χ_M') and out-of-phase (χ_M'') susceptibility signals were strongly frequency dependent with a maximum between 2.8–3.2 K and 2–3 K, respectively, which are accompanied by the increase of peak temperature as well as the decrease of the peak height of χ_M' with increasing temperature while the maximum of the χ_M'' peaks shifts to lower temperature with decreasing frequencies. Such a shift of the maximum of χ_M' and χ_M'' in temperature with frequency is a positive signature of a SMM, a single chain magnetism (SCM), a spin glass or a superparamagnetic behavior.[30d,33,34] In order to gain insight into the real magnetic behavior of **1**, we first tried to determine the relaxation time. The peak temperature (T_p) of χ_M'' abides fairly closely to the Arrhenius law $\tau = \tau_0 \exp(\Delta E/k_B T_p)$ with a linear correlation of $\ln(1/\tau)$ *vs.* $1/T_p$ ($\tau = 1/2\pi f$), resulting in the relaxation time $\tau_0 = 8.6 \times 10^{-27}$ s and the energy barrier $\Delta E/k_B$ = 138.6 K (Fig. 10a). The rather small value of τ_0 is obtained beyond the normal range of typical SMMs or SCMs (10^{-7}–10^{-12} s),[35] excluding the possibility of SMM and SCM behavior in **1**.[33] The parameter $\phi = \Delta T_p/[T_p \Delta(\log f)]$, as a quantitative measurement of the frequency-dependent peak temperature shift (ΔT_p) of χ_M'', is acquired as 0.045 and lies in the region of normal spin-glass behavior, indicating that **1** has spin-glass behavior. This also precludes the possibility of **1** as a superparamagnet because the ϕ value of 0.045 is much smaller than that of a superparamagnet.[33] Moreover, another quantitative measurement in a spin-glass system is also determined by fitting the frequency dependence maxima in χ_M'' using the conventional critical scaling law of the spin dynamics, $\tau = \tau_0[(T_p - T_f)/T_f]^{-zv}$,[36] where T_f and zv represent the freezing temperature and the critical exponent, respectively. The best-fitting

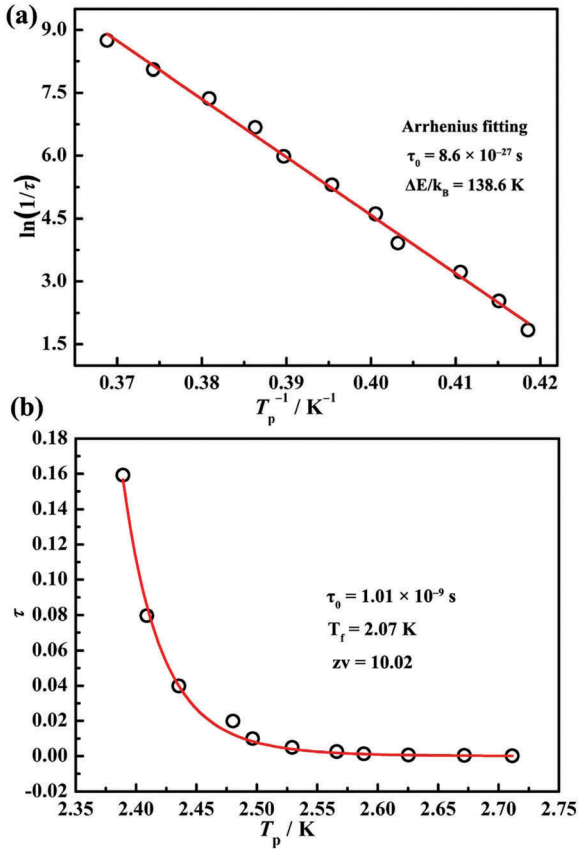

Fig. 10 (a) The Arrhenius fitting for **1**; (b) frequency dependence of ac χ_M'' of **1** fitted by the conventional critical scaling law of the spin dynamics as described by $\tau = \tau_0[(T_p - T_f)/T_f]^{-zv}$. The red lines are from the fitting results.

parameters were estimated to be $\tau_0 = 1.01 \times 10^{-9}$ s, $T_f = 2.07$ K and zv = 10.02 (Fig. 10b), and the zv value just falls in the typical range (4–12) of the conventional spin glasses.[33,34] All ac measurements and the deduced results are indicative of the canonical spin glass characteristic for **1**, which may probably be attributed to the intercluster couplings.[31a] Similar behaviors have been encountered in 1-D chain-like complexes such as $[Mn((R,R)\text{-salphen})Cr(Tp)(CN)_3]_n$ (Salphen = *N*,*N*′-1,2-diphenylethylene-bis(salicylideneiminato)dianion and Tp = tris(pyrazolyl)-hydroborate),[31a] $\{[Co^{II}_3(DMF)_{12}][W(CN)_8]_2\}_\infty$[34] and $[Fe(qcq)(CN)_3]$-$[Mn(salen)]\cdot MeCN\cdot H_2O$ (salen = *N*,*N*′-ethylenebis (salicylideneiminato)dianion).[37] As far as we know, **1** is the first tungstoantimonate-based material showing the coexistence of long-range FM ordering and spin-glass behavior.

Chemists have not only been pushing to assemble larger POM species with higher-nuclear TM cores, but are also attempting to design anticipated magnetic materials with novel structures. For instance, Fe-substituted POMs show possible spin-crossover magnetic features arising from the large number of unpaired electrons in the high-spin $Fe^{II/III}$ ions,[38] and Mn-substituted POMs are of great interest in the SMM materials derived from large magnetic anisotropy favored by the high valence states of Mn ions.[12,18] Among magnetic TMSPs, the FM, AFM and SMM behaviors are the most common, however, other interesting magnetic phenomena are rarely reported. Only in 2004, an unusual spin glass behavior was discovered by Zhu *et al.* in a 1-D mixed molybdenum–vanadium polymer $\{[Ni(phen)_2(H_2O)]_2$-$[Ni(phen)_2][V^{IV}_8Mo^{VI}_6Mo^{V}_2O_{40}(PO_4)]\}\{[Ni(phen)_2(H_2O)]_2[VI^{V}_8Mo^{VI}$-$Mo^{V}_2O_{40}(PO_4)_2]\}\cdot 5H_2O\cdot 2EtOH$ (phen = 1,10-phenanthroline and EtOH = ethanol) that was prepared under hydrothermal conditions.[39] However, no great development involving spin-glass behavior was made in TMSP chemistry in the past several years until the isolation of **1**. The intensive investigations on the spin-glass behavior of **1** not only illustrate the importance of the intercluster couplings leading to spin-glass behavior, but also can provide some valuable information for further designing and discovering novel POM-based magnetic materials in the future. In addition, the magnetic observation of **1** can also exemplify the statement of Mydosh that intercluster couplings must be added to take into account spin glasses because the spin glass is not a non-interacting collection of clusters.[33]

Conclusions

In summary, we further developed the synthetic concept that utilizing extraneous flexible small organic carboxylate ligands as SSAs can capture *in situ* generated high-nuclear TM aggregates from the inductive effect of lacunary POM fragments to construct novel inorganic–organic hybrid high-nuclear STMSPs and thus prepared a novel inorganic–organic hybrid 1-D chain heteropolyoxotungstate **1** established by nona-Mn^{II}-sandwiched TA units and double Mn–C_2O_4 linkers. Above all, the coexistence of long-range FM ordering and spin-glass behavior has been observed in **1**, and to our knowledge, **1** represents the first 1-D nona-Mn^{II}-sandwiched TA displaying the coexistence of long-range FM ordering and spin glass characteristics. The successful preparation of **1** not only has great significance in the directed assembly of inorganic–organic hybrid high-nuclear magnetic TMSP materials, but also can largely expand the functional applications of POMs in the realm of molecular magnetic materials. Our further work will be focused on the following four aspects: (i) judicious selection and manipulation of appropriate oxidizing agents in the Mn/POM system to modulate variation of the chemical valence states of Mn ions allows for greater possibility in discovering new POM-based materials with interesting magnetic phenomena; (ii) other functional conjugated carboxylic acid ligands will be purposefully employed to propagate the elaborate and diverse TMSP fragments into polynuclear oligomers, polymeric aggregates and multidimensional sheets or frameworks and can effectively tune the magnetic exchange interactions between TM centers; (iii) RE ions have significant magnetic anisotropy resulting from their large unquenched orbital angular momentum, thereby, RE ions will be introduced to this family and affect the whole magnetic behaviors, giving rise to intriguing RE–TM heterometallic cluster-based materials with large magnetic anisotropy and high-spin states; (iv) the better understanding of the reliable relationship between structures and magnetic properties is extremely important so as to provide enlightening and valuable guidance for designing and controlling new cluster-based magnetic materials.

Acknowledgements

This work was supported by the Natural Science Foundation of China (21301049, U1304208, 21571048, and 21671054), the Program for Science & Technology Innovation Talents in Universities of Henan Province (16HASTIT001), the Innovation Scientists and Technicians Troop Construction Projects of Henan Province (174100510016), the Foundation of Education Department of Henan Province (16A150027), the Postdoctoral Foundation of Henan Province (20140025), the Foundation of State Key Laboratory of Structural Chemistry (20160016), the 2014 Special Foundation for Scientific Research Project of Henan University (XXJC20140001), the 2012 Young Backbone Teachers Foundation from Henan Province (2012GGJS-027), the Foundation of Education Department of Henan Province (16A150027) and the Students Innovative Pilot Plan of Henan University (15NA002 and 16NA005).

References

1 (*a*) S. V. Eliseeva and J.-C. G. Bunzli, *New J. Chem.*, 2011, **35**, 1165; (*b*) L. Bogani and W. Wernsdorfer, *Nat. Mater.*, 2008, **7**, 179; (*c*) R. Sessoli, *Angew. Chem., Int. Ed.*, 2012, **51**, 43.

2 (*a*) I. V. Kozhevnikov, *Chem. Rev.*, 1998, **98**, 171; (*b*) S.-S. Wang and G.-Y. Yang, *Chem. Rev.*, 2015, **115**, 4893; (*c*) J. T. Rhule, C. L. Hill and D. A. Judd, *Chem. Rev.*, 1998, **98**, 327; (*d*) J. M. Clemente-Juan, E. Coronado and A. Gaita-Ariño, *Chem. Soc. Rev.*, 2012, **41**, 7464; (*e*) S.-T. Zheng and G.-Y. Yang, *Chem. Soc. Rev.*, 2012, **41**, 7623; (*f*) E. Coronado and C. J. Gómez-García, *Chem. Rev.*, 1998, **98**, 273; (*g*) X. Ma, H. L. Li, L. J. Chen and J. W. Zhao, *Dalton Trans.*, 2016, **45**, 4935.

3 (*a*) B. S. Bassil, M. H. Dickman, M. Reicke, U. Kortz, B. Keita and L. Nadjo, *Dalton Trans.*, 2006, 4253; (*b*) N. Belai and M. T. Pope, *Chem. Commun.*, 2005, 5760; (*c*) D. Zhang, Y. Zhang, J. Zhao, P. Ma, J. Wang and J. Niu, *Eur. J. Inorg. Chem.*, 2013, 1672; (*d*) R. Sato, K. Suzuki, T. Minato, M. Shinoe, K. Yamaguchi and N. Mizuno, *Chem. Commun.*, 2015, **51**, 4081; (*e*) W.-C. Chen, C. Qin, X.-L. Wang, K.-Z. Shao, Z.-M. Su and E.-B. Wang, *Cryst. Growth Des.*, 2016, **16**, 2481.

4 (*a*) B. Botar and P. Kögerler, *Dalton Trans.*, 2008, 3150; (*b*) N. H. Nsouli, S. S. Mal, M. H. Dickman, U. Kortz, B. Keita, L. Nadjo and J. M. Clemente-Juan, *Inorg. Chem.*, 2007, **46**, 8763; (*c*) Y. Kikukawa, K. Suzuki, K. Yamaguchi and N. Mizuno, *Inorg. Chem.*, 2013, **52**, 8644; (*d*) S. Yao, Z. M. Zhang, Y. G. Li and E. B. Wang, *Aust. J. Chem.*, 2010, **63**, 96; (*e*) C. Pichon, A. Dolbecq, P. Mialane, J. Marrot, E. Rivière, M. Goral, M. Zynek, T. McCormac, S. A. Borshch, E. Zueva and F. Sécheresse, *Chem. – Eur. J.*, 2008, **14**, 3189; (*f*) R. J. Errington, G. Harle, W. Clegg and R. W. Harrington, *Eur. J. Inorg. Chem.*, 2009, 5240; (*g*) R. S. Winter, D.-L. Long and L. Cronin, *Inorg. Chem.*, 2015, **54**, 4151; (*h*) C. Ritchie, F. Li, C. P. Pradeep, D. Long, L. Xu and L. Cronin, *Dalton Trans.*, 2009, 6483; (*i*) Y. Hou, L. Xu, M. J. Cichon, S. Lense, K. I. Hardcastle and C. L. Hill, *Inorg. Chem.*, 2010, **49**, 4125; (*j*) L. Ruhlmann, J. Canny, R. Contant and R. Thouvenot, *Inorg. Chem.*, 2002, **41**, 3811; (*k*) X. Zhang, T. M. Anderson, Q. Chen and C. L. Hill, *Inorg. Chem.*, 2001, **40**, 418; (*l*) D. Gabb, C. P. Pradeep, H. N. Miras, S. G. Mitchell, D. Long and L. Cronin, *Dalton Trans.*, 2012, **41**, 10000.

5 (*a*) P. Mialane, J. Marrot, E. Riviére, J. Nebout and G. Hervé, *Inorg. Chem.*, 2001, **40**, 44; (*b*) R. Al-Oweini, B. S. Bassil, T. Palden, B. Keita, Y. H. Lan, A. K. Powell and U. Kortz, *Polyhedron*, 2013, **52**, 461; (*c*) J.-D. Compain, P. Mialane, A. Dolbecq, I. M. Mbomekallé, J. Marrot, F. Sécheresse, C. Duboc and E. Rivière, *Inorg. Chem.*, 2010, **49**, 2851; (*d*) L. Han, P.-P. Zhang, H.-S. Liu, H.-J. Pang, Y. Chen and J. Peng, *J. Cluster Sci.*, 2010, **21**, 81; (*e*) B. Botar, A. Ellern and P. Kögerler, *Dalton Trans.*, 2009, 5606; (*f*) N. H. Nsouli, A. H. Ismail, I. S. Helgadottir, M. H. Dickman, J. M. Clemente-Juan and U. Kortz, *Inorg. Chem.*, 2009, **48**, 5884; (*g*) S. G. Mitchell, C. Ritchie, D. L. Long and L. Cronin, *Dalton Trans.*, 2008, 1415; (*h*) T. M. Anderson, K. I. Hardcastle, N. Okun and C. L. Hill, *Inorg. Chem.*, 2001, **40**, 6418; (*i*) N. Laronze, J. Marrot and G. Hervé, *Inorg. Chem.*, 2003, **42**, 5857; (*j*) J. P. Wang, P. T. Ma, J. Li, H. Y. Niu and J. Y. Niu, *Chem. – Asian J.*, 2008, **3**, 822; (*k*) L.-H. Bi, U. Kortz, B. Keita, L. Nadjo and L. Daniels, *Eur. J. Inorg. Chem.*, 2005, 3034; (*l*) A. C. Stowe, S. Nellutla, N. S. Dalal and U. Kortz, *Eur. J. Inorg. Chem.*, 2004, 3792; (*m*) L.-H. Bi, M. Reicke, U. Kortz, B. Keita, L. Nadjo and R. J. Clark, *Inorg. Chem.*, 2004, **43**, 3915; (*n*) U. Kortz, N. K. Al-Kassem, M. G. Savelieff, N. A. Al Kadi and M. Sadakane, *Inorg. Chem.*, 2001, **40**, 4742; (*o*) H. Liu, C. Qin, Y.-G. Wei, L. Xu, G.-G. Gao, F.-Y. Li and X.-S. Qu, *Inorg. Chem.*, 2008, **47**, 4166; (*p*) I. M. Mbomekalle, B. Keita, L. Nadjo, W. A. Neiwert, L. Zhang, K. I. Hardcastle, C. L. Hill and T. M. Anderson, *Eur. J. Inorg. Chem.*, 2003, 3924; (*q*) D. Schaming, J. Canny, K. Boubekeur, R. Thouvenot and L. Ruhlmann, *Eur. J. Inorg. Chem.*, 2009, 5004; (*r*) T. M. Anderson, X. Zhang, K. I. Hardcastle and C. L. Hill, *Inorg. Chem.*, 2002, **41**, 2477; (*s*) I. M. Mbomekalle, B. Keita, M. Nierlich, U. Kortz, P. Berthet and L. Nadjo, *Inorg. Chem.*, 2003, **42**, 5143; (*t*) B. Keita, I. M. Mbomekalle, L. Nadjo, T. M. Anderson and C. L. Hill, *Inorg. Chem.*, 2004, **43**, 3257; (*u*) J. M. Clemente-Juan, E. Coronado, A. Gaita-Ariño, C. Giménez-Saiz, H.-U. Güdel, A. Sieber, R. Bircher and H. Mutka, *Inorg. Chem.*, 2005, **44**, 3389; (*v*) U. Kortz, I. M. Mbomekalle, B. Keita, L. Nadjo and P. Berthet, *Inorg. Chem.*, 2002, **41**, 6412; (*w*) M. Lebrini, I. M. Mbomekallé, A. Dolbecq, J. Marrot, P. Berthet, J. Ntienoue, F. Sécheresse, J. Vigneron and A. Etcheberry, *Inorg. Chem.*, 2011, **50**, 6437; (*x*) G. B. Zhu, Y. V. Geletii, J. Song, C. C. Zhao, E. N. Glass, J. Bacsa and C. L. Hill, *Inorg. Chem.*, 2013, **52**, 1018.

6 (*a*) K. Suzuki, Y. Kikukawa, S. Uchida, H. Tokoro, K. Imoto, S. Ohkoshi and N. Mizuno, *Angew. Chem., Int. Ed.*, 2012, **51**, 1597; (*b*) Y. Liu, B. Liu, G. Xue, H. Hu, F. Fu and J. Wang, *Dalton Trans.*, 2007, 3634; (*c*) L. Ruhlmann, C. Costa-Coquelard, J. Canny and R. Thouvenot, *Eur. J. Inorg. Chem.*, 2007, 1493; (*d*) G. Zhu, Y. V. Geletii, P. Kögerler, H. Schilder, J. Song, S. Lense, C. Zhao, K. I. Hardcastle, D. G. Musaev and C. L. Hill, *Dalton Trans.*, 2012, **41**, 2084;

(*e*) Z. Luo, P. Kögerler, R. Cao, I. Hakim and C. L. Hill, *Dalton Trans.*, 2008, 54; (*f*) H. Liu, C. J. Gómez-García, J. Peng, Y. Feng, Z. Su, J. Sha and L. Wang, *Inorg. Chem.*, 2007, **46**, 10041; (*g*) U. Kortz, M. G. Savelieff, B. S. Bassil, B. Keita and L. Nadjo, *Inorg. Chem.*, 2002, **41**, 783; (*h*) I. M. Mbomekalle, B. Keita, L. Nadjo, P. Berthet, K. I. Hardcastle, C. L. Hill and T. M. Anderson, *Inorg. Chem.*, 2003, **42**, 1163; (*i*) L. Chen, K. Zhu, L. H. Bi, A. Suchopar, M. Reicke, G. Mathys, H. Jaensch, U. Kortz and R. M. Richards, *Inorg. Chem.*, 2007, **46**, 8457; (*j*) L. H. Bi, E. B. Wang, J. Peng, R. D. Huang, L. Xu and C. W. Hu, *Inorg. Chem.*, 2000, **39**, 671; (*k*) J. M. Clemente, H. Andres, M. Aebersold, J. J. Borrás-Almenar, E. Coronado, H. U. Güdel, H. Buttner and G. Kearly, *Inorg. Chem.*, 1997, **36**, 2244; (*l*) N. H. Nsouli, M. Prinz, N. Damnik, M. Neumann, E. Talik and U. Kortz, *Eur. J. Inorg. Chem.*, 2009, 5096; (*m*) J. Wang, P. Ma, Y. Shen and J. Niu, *Cryst. Growth Des.*, 2008, **8**, 3130; (*n*) I. M. Mbomekalle, B. Keita, L. Nadjo, K. I. Hardcastle, C. L. Hill and T. M. Anderson, *Dalton Trans.*, 2004, 4094; (*o*) P. Mialane, C. Duboc, J. Marrot, E. Rivière, A. Dolbecq and F. Sécheresse, *Chem. – Eur. J.*, 2006, **12**, 1950; (*p*) J. W. Zhao, B. Li, S. T. Zheng and G. Y. Yang, *Cryst. Growth Des.*, 2007, **7**, 2658; (*q*) B. Botar, P. Kögerler and C. L. Hill, *Inorg. Chem.*, 2007, **46**, 5398; (*r*) A. Dolbecq, J.-D. Compain, P. Mialane, J. Marrot, E. Rivière and F. Sécheresse, *Inorg. Chem.*, 2008, **47**, 3371; (*s*) U. Kortz, S. Nellutla, A. C. Stowe, N. S. Dalal, J. van Tol and B. S. Bassil, *Inorg. Chem.*, 2004, **43**, 144.

7 (*a*) L. H. Bi and U. Kortz, *Inorg. Chem.*, 2004, **43**, 7961; (*b*) H. Andres, J. M. Clemente-Juan, R. Basler, M. Aebersold, H. U. Güdel, J. J. Borrás-Almenar, A. Gaita, E. Coronado, H. Büttner and S. Janssen, *Inorg. Chem.*, 2001, **40**, 1943; (*c*) Z. M. Zhang, E. B. Wang, Y. F. Qi, Y. G. Li, B. D. Mao and Z. M. Su, *Cryst. Growth Des.*, 2007, **7**, 1305; (*d*) K. Suzuki, R. Sato, T. Minato, M. Shinoe, K. Yamaguchi and N. Mizuno, *Dalton Trans.*, 2015, **44**, 14220.

8 (*a*) J. P. Wang, P. T. Ma, Y. Shen and J. Y. Niu, *Cryst. Growth Des.*, 2007, **7**, 603; (*b*) J. D. Compain, P. Mialane, A. Dolbecq, I. M. Mbomekallé, J. Marrot, F. Sécheresse, E. Rivière, G. Rogez and W. Wernsdorfer, *Angew. Chem., Int. Ed.*, 2009, **48**, 3077; (*c*) T. M. Anderson, R. Cao, W. A. Neiwert, K. I. Hardcastle, C. L. Hill, M. Ammam, B. Keita and L. Nadjo, *Eur. J. Inorg. Chem.*, 2005, 1770; (*d*) T. M. Anderson, W. A. Neiwert, K. I. Hardcastle and C. L. Hill, *Inorg. Chem.*, 2004, **43**, 7353; (*e*) L.-H. Bi, U. Kortz, S. Nellutla, A. C. Stowe, J. Tol, N. S. Dalal, B. Keita and L. Nadjo, *Inorg. Chem.*, 2005, **44**, 896; (*f*) Z. M. Zhang, Y. G. Li, E. B. Wang, X. L. Wang, C. Qin and H. Y. An, *Inorg. Chem.*, 2006, **45**, 4313; (*g*) S. T. Zheng, D. Q. Yuan, J. Zhang and G. Y. Yang, *Inorg. Chem.*, 2007, **46**, 4569; (*h*) J.-W. Zhao, S.-T. Zheng, Z.-H. Li and G.-Y. Yang, *Dalton Trans.*, 2009, 1300; (*i*) C. Ritchie, A. Ferguson, H. Nojiri, H. N. Miras, Y.-F. Song, D.-L. Long, E. Burkholder, M. Murrie, P. Kögerler, E. K. Brechin and L. Cronin, *Angew. Chem., Int. Ed.*, 2008, **47**, 5609; (*j*) C. Lydon, C. Busche, H. N. Miras, A. Delf, D.-L. Long, L. Yellowlees and L. Cronin, *Angew. Chem., Int. Ed.*, 2012, **51**, 2115; (*k*) T. Yamase, K. Fukaya, H. Nojiri and Y. Ohshima, *Inorg. Chem.*, 2006, **45**, 7698; (*l*) H. Xue, J.-W. Zhao, R. Pan, B.-F. Yang, G.-Y. Yang and H.-S. Liu, *Chem. – Eur. J.*, 2016, **22**, 12322; (*m*) W.-C. Chen, C. Qin, X.-L. Wang, Y.-G. Li, H.-Y. Zang, Y.-Q. Jiao, P. Huang, K.-Z. Shao, Z.-M. Su and E.-B. Wang, *Chem. Commun.*, 2014, **50**, 13265; (*n*) L.-Y. Guo, S.-Y. Zeng, Z. Jagličić, Q.-D. Hu, S.-X. Wang, Z. Wang and D. Sun, *Inorg. Chem.*, 2016, **55**, 9006; (*o*) Z. Zhao, B. Zhou, S. Zheng, Z. Su and C. Wang, *Inorg. Chim. Acta*, 2009, **362**, 5038.

9 (*a*) J. W. Zhao, D. Y. Shi, L. J. Chen, X. M. Cai, Z. Q. Wang, P. T. Ma, J. P. Wang and J. Y. Niu, *CrystEngComm*, 2012, **14**, 2797; (*b*) H. Moll, A. Dolbecq, J. Marrot, G. Rousseau, M. Haouas, F. Taulelle, G. Rogez, W. Wernsdorfer, B. Keita and P. Mialane, *Chem. – Eur. J.*, 2012, **18**, 3845.

10 (*a*) J. W. Zhao, H. P. Jia, J. Zhang, S. T. Zheng and G. Y. Yang, *Chem. – Eur. J.*, 2007, **13**, 10030; (*b*) J.-W. Zhao, C.-M. Wang, J. Zhang, S.-T. Zheng and G.-Y. Yang, *Chem. – Eur. J.*, 2008, **14**, 9223; (*c*) J.-W. Zhao, J. Zhang, S.-T. Zheng and G.-Y. Yang, *Chem. Commun.*, 2008, 570; (*d*) L. Lisnard, P. Mialane, A. Dolbecq, J. Marrot, J. Clemente-Juan, E. Coronado, B. Keita, P. Oliveira, L. Nadjo and F. Sécheresse, *Chem. – Eur. J.*, 2007, **13**, 3525.

11 (*a*) C. Pichon, P. Mialane, A. Dolbecq, J. Marrot, E. Rivière, B. S. Bassil, U. Kortz, B. Keita, L. Nadjo and F. Sécheresse, *Inorg. Chem.*, 2008, **47**, 11120; (*b*) Z. Zhou, D. D. Zhang, L. Yang, P. T. Ma, Y. N. Si, U. Kortz, J. Y. Niu and J. P. Wang, *Chem. Commun.*, 2013, **49**, 5189.

12 Z.-M. Zhang, S. Yao, Y.-G. Li, H.-H. Wu, Y.-H. Wang, M. Rouzières, R. Clérac, Z.-M. Su and E.-B. Wang, *Chem. Commun.*, 2013, **49**, 2515.

13 V. Singh, Z. Y. Chen, P. T. Ma, D. D. Zhang, M. G. B. Drew, J. Y. Niu and J. P. Wang, *Chem. – Eur. J.*, 2016, **22**, 10983.

14 J. Fischer, L. Richard and R. Weiss, *J. Am. Chem. Soc.*, 1976, **98**, 3050.

15 (*a*) I. Loose, E. Droste, M. Bösing, H. Pohlmann, M. H. Dickman, C. Rosu, M. T. Pope and B. Krebs, *Inorg. Chem.*, 1999, **38**, 2688; (*b*) M. Piepenbrink, E. M. Limanski and B. Krebs, *Z. Anorg. Allg. Chem.*, 2002, **628**, 1187; (*c*) M. H. Sun, F. Y. Li, L. J. Yu, Y. Wang and L. Xu, *Dalton Trans.*, 2016, **45**, 2417.

16 (*a*) B. Artetxe, S. Reinoso, L. S. Felices, P. Vitoria, A. Pache, J. Martín-Caballero and J. M. Gutierrez-Zorrilla, *Inorg. Chem.*, 2015, **54**, 241; (*b*) D. Laurencin, R. Villanneau, P. Herson, R. Thouvenot, Y. Jeannin and A. Proust, *Chem. Commun.*, 2005, 5524; (*c*) L. H. Bi, G. Al-Kadamany, E. V. Chubarova, M. H. Dickman, L. F. Chen, D. S. Gopala, R. M. Richards, B. Keita, L. Nadjo, H. Jaensch, G. Mathys and U. Kortz, *Inorg. Chem.*, 2009, **48**, 10068.

17 (*a*) X. Q. Du, Y. Ding, F. Y. Song, B. C. Ma, J. W. Zhao and J. Song, *Chem. Commun.*, 2015, **51**, 13925; (*b*) B. Artetxe, S. Reinoso, L. S. Felices, L. Lezama, A. Pache, C. Vicent and J. M. Gutierrez-Zorrilla, *Inorg. Chem.*, 2015, **54**, 409; (*c*) O. Oms, S. Yang, W. Salomon, J. Marrot, A. Dolbecq, E. Rivière, A. Bonnefont, L. Ruhlmann and P. Mialane, *Inorg. Chem.*, 2016, **55**, 1551; (*d*) Z.-M. Zhang, X. P. Duan, S. Yao, Z. S. Wang, Z. K. Lin, Y.-G. Li, L.-S. Long, E.-B. Wang and W. B. Lin, *Chem. Sci.*, 2016, **7**, 4220; (*e*) Z.-G. Han, H.-X. Zhang, D.-S. Zhang, C.-N. Liu, R. Zheng, G.-B. Xia and X.-X. Wang, *Inorg. Chem.*, 2016, **55**, 12488.

18 (*a*) X. K. Fang, M. Speldrich, H. Schilder, R. Cao, K. P. O'Halloran, C. L. Hill and P. Kögerler, *Chem. Commun.*, 2010, **46**, 2760; (*b*) X. Fang, K. McCallum, H. D. Pratt III, T. M. Anderson, K. Dennis and M. Luban, *Dalton Trans.*, 2012, **41**, 9867.

19 M. Bösing, I. Loose, H. Pohlmann and B. Krebs, *Chem. – Eur. J.*, 1997, **3**, 1232.

20 G. M. Sheldrick, *SADABS: Program for Empirical Absorption Correction of Area Detector Data*, University of Göttingen, Germany, 1996.

21 (*a*) G. M. Sheldrick, *SHELXS 97, Program for Crystal Structure Solution*, University of Göttingen, Germany, 1997; (*b*) G. M. Sheldrick, *SHELXL 97, Program for Crystal Structure Refinement*, University of Göttingen, Germany, 1997.

22 I. D. Brown and D. Altermatt, *Acta Crystallogr., Sect. B: Struct. Sci.*, 1985, **41**, 244.

23 (*a*) H. Martinez, A. Benayad, D. Gonbeau, P. Vinatier, B. Pecquenard and A. Levasseur, *Appl. Surf. Sci.*, 2004, **236**, 377; (*b*) W. C. Chen, H. L. Li, X. L. Wang, K. Z. Shao, Z. M. Su and E. B. Wang, *Chem. – Eur. J.*, 2013, **19**, 11007.

24 (*a*) Y. F. Han, F. X. Chen, Z. Y. Zhong, K. Ramesh, L. W. Chen and E. Widjaja, *J. Phys. Chem. B*, 2006, **110**, 24450; (*b*) V. Di Castro and G. Polzonetti, *J. Electron Spectrosc. Relat. Phenom.*, 1989, **48**, 117.

25 T. Honma, R. Sato, Y. Benino, T. Komatsu and V. Dimitrov, *J. Non-Cryst. Solids*, 2000, **272**, 1.

26 B. Li, J.-W. Zhao, S.-T. Zheng and G.-Y. Yang, *Inorg. Chem.*, 2009, **48**, 8294.

27 B. Modec, D. Dolenc and M. Kasunič, *Inorg. Chem.*, 2008, **47**, 3625.

28 (*a*) C. H. Li, K. L. Huang, Y. N. Chi, X. Liu, Z. G. Han, L. Shen and C. W. Hu, *Inorg. Chem.*, 2009, **48**, 2010; (*b*) H. An, Z. Han and T. Xu, *Inorg. Chem.*, 2010, **49**, 11403; (*c*) K. Nakamoto, *Infrared and Raman Spectra of Inorganic and Coordination Compounds*, John Wiley and Sons, New York, 3rd edn, 1978.

29 (*a*) J. M. Clemente-Juan and E. Coronado, *Coord. Chem. Rev.*, 1999, **193–195**, 361; (*b*) N. Zamstein, A. Tarantul and B. Tsukerblat, *Inorg. Chem.*, 2007, **46**, 8851.

30 (*a*) D. Deguenon, G. Bernardinelli, J. P. Tuchagues and P. Castan, *Inorg. Chem.*, 1990, **29**, 3031; (*b*) J. Glerup, P. A. Goodson, D. J. Hodgson and K. Michelsen, *Inorg. Chem.*, 1995, **34**, 6255; (*c*) U. García-Couceiro, O. Castillo, A. Luque, J. P. García-Terán, G. Beobide and P. Román, *Cryst. Growth Des.*, 2006, **6**, 1839; (*d*) Z.-X. Wang, X.-L. Li, T.-W. Wang, Y.-Z. Li, S. Ohkoshi, K. Hashimoto, Y. Song and X.-Z. You, *Inorg. Chem.*, 2007, **46**, 10990.

31 (*a*) M.-X. Yao, Q. Zheng, X.-M. Cai, Y.-Z. Li, Y. Song and J.-L. Zuo, *Inorg. Chem.*, 2012, **51**, 2140; (*b*) W. Liu, C.-F. Wang, Y.-Z. Li, J.-L. Zuo and X.-Z. You, *Inorg. Chem.*, 2006, **45**, 10058; (*c*) X.-T. Liu, X.-Y. Wang, W.-X. Zhang, P. Cui and S. Gao, *Adv. Mater.*, 2006, **18**, 2852.

32 (*a*) O. Kahn, *Molecular Magnetism*, VCH, Weinheim, Germany, 1993; (*b*) R. L. Carlin and A. J. van Duyneveldt, *Magnetic Properties of Transition Metal Compounds*, Springer, New York, 1977.

33 J. A. Mydosh, *Spin Glasses: An Experimental Introduction*, Taylor & Francis, London, 1993.

34 D. F. Li, L. M. Zheng, Y. Z. Zhang, J. Huang, S. Gao and W. X. Tang, *Inorg. Chem.*, 2003, **42**, 6123.

35 R. Clérac, H. Miyasaka, M. Yamashita and C. Coulon, *J. Am. Chem. Soc.*, 2002, **124**, 12837.

36 (*a*) Y.-Z. Zheng, M.-L. Tong, W.-X. Zhang and X.-M. Chen, *Angew. Chem., Int. Ed.*, 2006, **45**, 6310; (*b*) X.-J. Li, X.-Y. Wang, S. Gao and R. Cao, *Inorg. Chem.*, 2006, **45**, 1508.

37 J. I. Kim, H. Y. Kwak, J. H. Yoon, D. W. Ryu, I. Y. Yoo, N. Yang, B. K. Cho, J. G. Park, H. Lee and C. S. Hong, *Inorg. Chem.*, 2009, **48**, 2956.

38 (*a*) O. Sato, *Acc. Chem. Res.*, 2003, **36**, 692; (*b*) V. Ksenofontov, A. B. Gaspar, V. Niel, S. Reiman, J. A. Real and P. Gütlich, *Chem. – Eur. J.*, 2004, **10**, 1291.

39 C.-M. Liu, J.-L. Luo, D.-Q. Zhang, N.-L. Wang, Z.-J. Chen and D.-B. Zhu, *Eur. J. Inorg. Chem.*, 2004, 4774.